

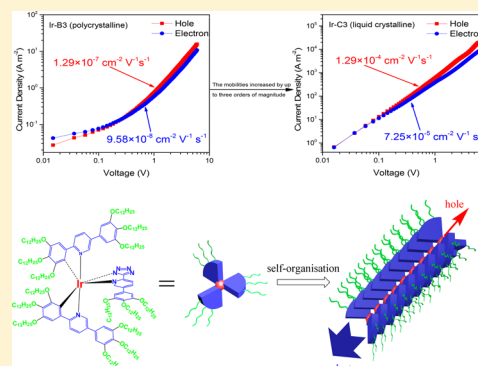
Columnar Iridium(III) Metallomesogens Based on Polycatenar Pyridyltetrazolate with Ambipolar Carrier Mobility Behavior

Guo Zou, Li Zhao, Longwei Zeng, Kaijun Luo,*¹ Hailiang Ni, Haifeng Wang, Quan Li, Wenhao Yu, and Xuelian Li

College of Chemistry and Materials Science, Sichuan Normal University, 5 Jingan Road, Chengdu 610068, China

S Supporting Information

ABSTRACT: In this paper, we have designed and synthesized a series of neutral liquid-crystalline iridium(III) complexes based on polycatenar 2,5-diphenylpyridine and pyridyltetrazolate derivatives. Iridium(III) complexes all display highly emissive behavior with photoluminescence quantum yields in the range of 0.45–0.66 and a maximum emission wavelength at ~ 563 nm. Hexagonal columnar mesophases of iridium(III) complexes can be obtained by changing the number and length of peripheral alkoxy chains attached to a 2,5-diphenylpyridine ligand (main ligand) and a pyridyltetrazolate ligand (auxiliary ligand). Moreover, experimental results of the charge transport properties for these iridium(III) complexes, which were measured by the space charge limited-current method, exhibit ambipolar carrier mobility behavior. In particular, the liquid-crystalline iridium(III) complexes can self-organize into one-dimensional (1D) nanostructure after thermal annealing treatment in their liquid-crystalline phase. The devices based on liquid crystal film display improved charge transport behavior compared with that of the devices based on polycrystalline film, indicating 1D nanostructure is beneficial to charge carrier injection and transportation.



INTRODUCTION

In recent decades, iridium and platinum transition elements have been widely used in the synthesis of highly efficient luminescence materials.^{1–4} Because of the electron spin–orbit coupling and fast intersystem crossing, these heavy metal complexes can capture electrogenerated singlet and triplet excitons in the emitting layer of organic light-emitting diodes (OLEDs) and theoretically make their internal quantum efficiency $\leq 100\%$.^{1,3} Iridium(III) complexes have attracted a great deal of attention due to their many advantages, such as their high quantum efficiency, chemical stability, and flexibility in color tuning. Therefore, many related applications came into being, for example, OLEDs,^{4–9} light-emitting electrochemical cells (LECs),^{6,10,11} sensors,^{12,13} and biological imaging.^{14–17}

Metal-containing liquid crystals (metallomesogens) have also received a great deal of attention because of the improved carrier transportation and polarized emission in the liquid crystal phase.^{18–37} Compared with iridium(III) complexes, platinum(II) complexes have a square planar geometry and tend to become a class of mesogenic materials by connecting several flexible chains at the periphery of the molecules. However, the device based on platinum(II) complexes as an emitter often shows deteriorated device performance, showing a lower device efficiency and red-shifted luminescence, which result from strong intermolecular interactions of planar platinum(II) complexes.^{38,39} Although the devices fabricated by phosphorescent iridium(III) complexes can avoid these disadvantages, it is difficult to obtain liquid-crystalline

iridium(III) complexes because of their octahedral structure. Until now, a few iridium(III) metallomesogens have been reported.^{40–43}

Very recently, we reported the new lamellar platinum(II) metallomesogens consisting of rodlike 2-phenylpyridine and pyridyltetrazolate. These platinum(II) metallomesogens were found to have ambipolar charge transporting behavior upon the introduction of the pyridyltetrazolate unit with an electron affinity.⁴⁴ The results encouraged us to explore the possibility of obtaining iridium(III) metallomesogens with ambipolar charge transporting behavior by connecting polycatenar 2,5-diphenylpyridine with pyridyltetrazolate (Figure 1). The neutral iridium(III) complexes were obtained from the iridium(III) chloro-bridged dimers and pyridyltetrazolate derivatives. The iridium(III) chloro-bridged dimers were prepared according to a literature procedure,⁴¹ and pyridyltetrazolate derivatives were easily obtained by “click chemistry.”⁴⁵

EXPERIMENTAL SECTION

Materials and Methods. All commercially available starting materials were used directly without further purification. The solvents were carefully dried prior to use. ¹H nuclear magnetic resonance (NMR) and ¹³C NMR spectra were recorded on a Varian INOVA 400 MHz spectrometer. Elemental analyses were performed with a

Received: October 20, 2018

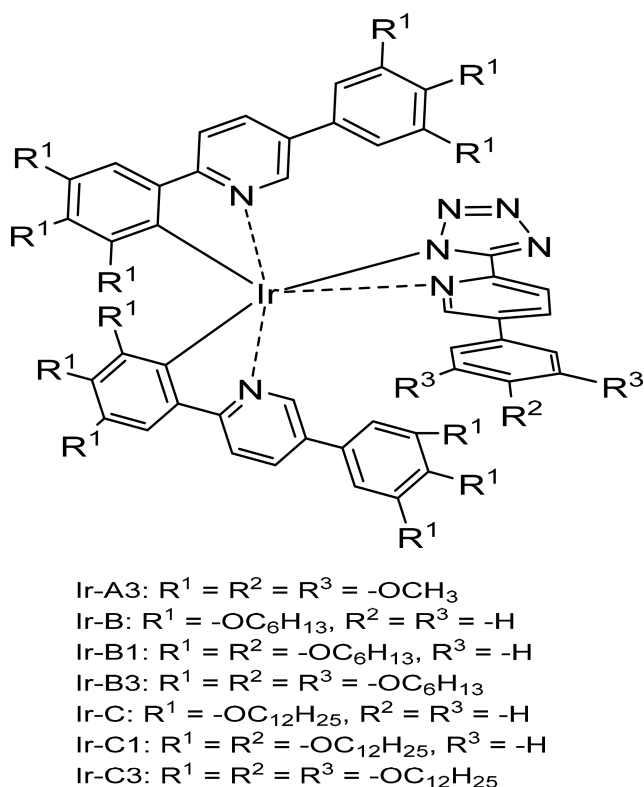


Figure 1. Chemical structures of all iridium(III) complexes.

Euro Vector EA300 element analyzer. Polarized optical microscopy (POM) was performed on an Olympus BX41 instrument. Differential scanning calorimetry (DSC) experiments were performed on a TA Discovery DSC instrument at a scan rate of 10 °C/min under the protection of nitrogen. X-ray diffraction (XRD) was measured on a Rigaku SmartLab (Cu $K\alpha$). Ultraviolet–visible absorption spectra were measured at room temperature on a PerkinElmer Lambda 950 spectrophotometer. The photoluminescence (PL) spectra at 298 and 77 K were measured on a Horiba Fluorolog-4 spectrophotometer. Dichloromethane (CH_2Cl_2) solutions ($M = 1.0 \times 10^{-5}$ mol/L) of samples were degassed by more than three freeze–pump–thaw cycles prior to measurement. Quantum efficiency measurements were taken at room temperature in CH_2Cl_2 solutions, and $[Ru(bpy)_3]Cl_2$ in a degassed aqueous solution (excitation wavelength of 436 nm; $\Phi_{lum} = 0.042$) was used as a reference.⁴⁶ The equation $\Phi_s = \Phi_r(A_r/A_s)(n_s/n_r)^2(I_s/I_r)$ was used to calculate the quantum yields, where Φ_s is the quantum yield of the sample, Φ_r is the quantum yield of the reference, A_s and A_r are the absorbance of the sample and the reference, respectively, at the wavelength of excitation, I_s and I_r are the integrated areas of emission bands, and n is the refractive index of the solvent (at 298 K, $n_s = 1.4244$ and $n_r = 1.3325$). The time-resolved measurements were taken on a Horiba Fluorolog-4 spectrophotometer to measure the excited state lifetime. Nano LED 370 ($\lambda = 370$ nm) was used as the excitation source, and the time-correlated single-photo count (TCSPC) method was used to collect photos.

X-ray Crystallographic Analysis. A New Gemini (Dual, Cu at zero) EosS2 diffractometer was used to collect single-crystal data at 150 K. The structure was determined by Olex2 with the Superflippogram and refined with the ShelXL package (least-squares minimization).^{47–49}

Electrochemical Tests. Electrochemical measurements were taken on an autolab PGSTAT302 voltammetric analyzer at room temperature in an anhydrous CH_2Cl_2 solution (the concentration of the samples was 1.0×10^{-3} mol/L) containing 0.1 mol/L tetrabutylammonium hexafluorophosphate (Bu_4NPF_6) as a supporting electrolyte at a scan rate of 100 mV s^{-1} . The solutions were carefully deaerated by high-purity argon bubbling before the scans.

Cyclic voltammograms were measured using the single-compartment three-electrode cell. A glassy carbon electrode was used for the working electrode. A Pt wire and a $Ag/AgNO_3$ (0.1 mol/L in dry acetonitrile) electrode were used as the counter electrode and the reference electrode, respectively. Bu_4NPF_6 was purified by recrystallization before being used. The glassy carbon electrode was polished with 0.5 μm diamond powder prior to use. All of the electrochemical data reported here were measured relative to an external ferrocene/ferrocenium reference (Fc/Fc^+).

Device Fabrication and Measurements. Hole-only devices were fabricated with an ITO/PEDOT:PSS (35 nm)/Ir–B3 or Ir–C3 (100 nm)/ MoO_3 (10 nm)/Au (100 nm) structure.^{50,51} First, glass substrates with prepatterned indium tin oxide (ITO, sheet resistance of 15 Ωsq^{-1}) were first ultrasonicated in a detergent, deionized water, acetone, and isopropanol and then modified by an ultraviolet–ozone treatment for 20 min. Second, poly(3,4-ethylenedioxythiophene):polystyrenesulfonate (PEDOT:PSS) was first filtered through a 0.45 μm nylon filter and then spin coated on the cleaned ITO substrates with a spin speed of 5000 rpm for 60 s to form a thin layer (35 nm). The substrates were baked on a hot plate at 140 °C for 15 min and transferred into the glovebox. Third, a film of Ir–B3 or Ir–C3 was prepared by the spin coating method from a solvent of CH_2Cl_2 with a concentration of 20 mg mL^{-1} at 1700 rpm for 60 s. Finally, a 10 nm MoO_3 layer was first evaporated onto the surface of the active blend before the evaporation of the Au (100 nm) electrode. Electron-only devices were fabricated with a glass/Al (100 nm)/Ir–B3 or Ir–C3 (100 nm)/Al (100 nm) structure; 100 nm of the Al electrode was evaporated before and after the active layer spin coating. The thickness of the films was measured using a Dektak 6 M surface profilometer. The active layers were heated to 150 °C for 5 min and then cooled slowly (5 °C/min) to room temperature. The device area was 0.04 cm^2 . The current density–voltage (I – V) characteristics were measured with a computer-controlled Keithley 2400 Source Measurement system. For the devices, the space charge limited current (SCLC) is described by the formula $J = (9/8)\epsilon_0\epsilon_r\mu(V^2/d^3)$,⁵⁰ where J is the current density, ϵ_0 is the permittivity under vacuum ($\epsilon_0 = 8.85 \times 10^{-12}$ F/m), ϵ_r is the dielectric constant ($\epsilon_r = 3$), μ is the charge mobility, and d is the thickness of the sample (100 nm).

RESULTS AND DISCUSSION

Crystal Structure of Ir–A3. Single crystals of Ir–A3 with methoxy chains, an analogue of polycatenar iridium(III) complexes, were obtained by slow evaporation of a chloroform/*n*-hexane solution of the complex at room temperature. The molecular structure is shown in Figure 2 (CCDC 1588649). The detailed crystallographic data and selected bond lengths and angles are summarized in Tables S1 and S2. Ir–A3 crystallizes in triclinic space group $P\bar{1}$. As shown in Figure 2, two cyclometalated 2,5-bis(3,4,5-trimethoxyphenyl)pyridine ligands and one 2-(1H-tetrazol-5-yl)-5-(3,4,5-trimethoxyphenyl)pyridine ligand coordinate with the central iridium(III) ion, forming a distorted octahedral structure around the central iridium atom, which is similar to the reported iridium(III) tetrazolate complexes reported previously.^{52,53} The aryl ring fragments of three ligands overlap partly in the steric configuration because of their anisotropic structures. Two carbon atoms and two nitrogen atoms of cyclometalated ligands exhibit *cis*-C–C and *trans*-N–N chelate dispositions, respectively. Ir–C bonds [2.039(4) and 2.049(4) Å] are slightly longer than those of similar iridium(III) tetrazolate complexes [1.991(19)–2.029(8) Å], and Ir–N bond lengths in the cyclometalated ligands and in the tetrazolate ligand are in the range of those of similar iridium(III) tetrazolate complexes [2.033(15)–2.064(7) and 2.096(7)–2.196(14) Å].^{52,53} The Ir–N distances in the auxiliary ligands {IrO1–N00M [2.183(3) Å] and IrO1–N00L

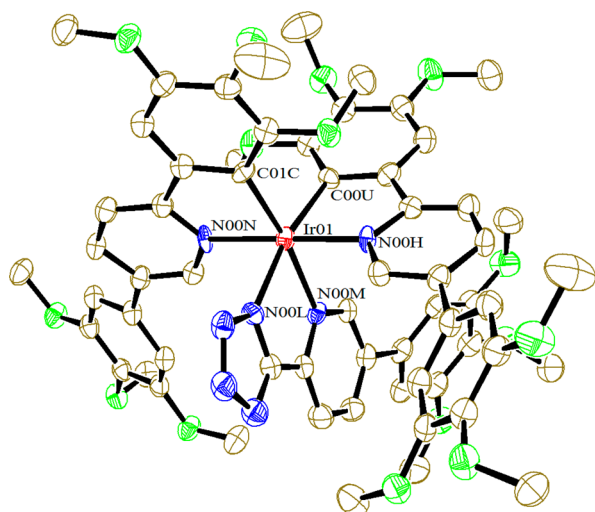


Figure 2. Perspective diagram of Ir-A3 with thermal ellipsoids shown at the 50% probability level. The hydrogen atoms have been omitted for the sake of clarity.

[2.125(3) Å]} are longer than those in cyclometalated ligands {Ir01–N00H [2.056(3) Å] and Ir01–N00N [2.064(3) Å]}. To minimize the steric effect and stabilize the crystal structure, three peripheral 3,4,5-trimethoxybenzene rings attached to two phenylpyridines and a pyridyltetrazolate moiety adopt the distorted configuration. The angles between two peripheral 3,4,5-trimethoxyphenyl and pyridyl groups of the main ligands are 42.58° and 30.54°, respectively, and the angle between the 3,4,5-trimethoxyphenyl and pyridyl group of the pyridyltetrazolate moiety is 30.48°. The shortest distance between the two iridium centers is 8.5331(5) Å in the crystal packing of Ir-A3.

Photophysical Properties. The ultraviolet–visible absorption and photoluminescence (PL) spectra of all iridium(III) complexes in degassed CH₂Cl₂ ($M = 1.0 \times 10^{-5}$ mol/L) are shown in Figure 3, and the corresponding photophysical data of all iridium(III) complexes are summarized in Table 1. The strong absorption bands in the ultraviolet region at approximately 220–350 nm, with molar extinction coefficients in the range of 18000–47000 M⁻¹ cm⁻¹, are assigned to the spin-allowed ligand-centered $\pi-\pi^*$ transitions (¹LC). In addition, because of the similar iridium(III) complexes previously reported^{5,8,53} and the results of time-dependent density functional theory calculations for Ir-A3 (vide infra), the weaker absorption bands centered at ~430 nm with molar extinction coefficients in the range of 3500–6900 M⁻¹ cm⁻¹ are tentatively attributed to the metal-to-ligand charge-transfer transitions (MLCT), with some mixture of ligand-centered $\pi-\pi^*$ transitions (LC). All iridium(III) complexes are highly luminescent in degassed CH₂Cl₂ solutions with a maximum emission wavelength at ~563 nm, accompanied by a shoulder peak at ~600 nm. These iridium(III) complexes exhibit nearly identical emission spectra with variation of only a few nanometers, indicating that the number and length of peripheral alkoxy chains have an only weak influence on the luminescence of molecules. Compared with similar liquid-crystalline iridium(III) complexes based on acac (Hacac is acetyl acetone) derivatives,⁴¹ these complexes exhibit luminescence that is blue-shifted by ~19 nm, showing that pyridyltetrazolate groups as auxiliary ligands have a certain effect on luminescence. Compared with PL spectra at room

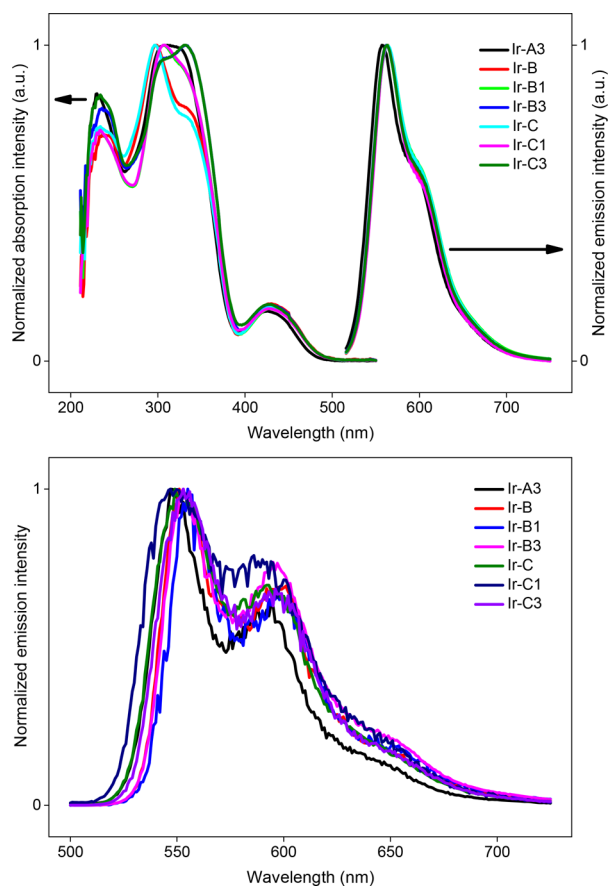


Figure 3. Photophysical spectra of iridium(III) complexes in degassed CH₂Cl₂ at room temperature (top) and 77 K (bottom) ($\lambda_{\text{ex}} = 425$ nm; $M = 1.0 \times 10^{-5}$ mol/L).

temperature, PL spectra of the the iridium(III) complexes show a blue-shift of 13 nm due to a rigidochromic effect at 77 K. The shoulder peak at ~600 nm becomes apparent, and the PL spectra show some structural characteristics at 77 K. In a degassed CH₂Cl₂ solution at room temperature, the PL quantum yields (Φ) of these iridium(III) complexes are in the range of 0.45–0.66 and higher than those of similar iridium(III) metallomesogens.^{40,52} The excited state lifetimes (τ) of all complexes are in the range of 0.21–0.27 μ s (Figure S1). Some structured PL spectra at 77 K and microsecond radiative lifetimes indicate the emission originates mainly from the excited state of MLCT with a certain contribution from the excited state of ³ $\pi-\pi^*$ transitions (³LC).^{53–57}

Moreover, the PL spectra of Ir-C1 and Ir-C3 complexes, in the liquid-crystalline phase (see below) and in the amorphous state, are very similar with peaks at ~578 nm (Figure S2 and Table S3) and displayed red-shifts of 15 nm from the CH₂Cl₂ solution to condensed phases, suggesting weaker intermolecular interactions in aggregation states.

Chirality is involved at different levels, such as subatomic, molecular, supramolecular, and macroscopic levels. Among these different levels, chirality at a molecular and supramolecular level is vitally important because it is strongly related to chemistry, physics, biology, materials, and nanoscience, which treat the matter on scales from atomic to molecular and supramolecular.⁵⁸ It has been known that nearly all the neutral iridium(III) complexes are racemic mixtures in solution,⁵⁹ but we would like to know whether Ir-C1 and Ir-C3 complexes

Table 1. Photophysical Data of Iridium(III) Complexes in Degassed CH₂Cl₂ ($\lambda_{\text{ex}} = 425 \text{ nm}$)

complex	absorption (nm) [ϵ ($\times 10^{-3} \text{ M}^{-1} \text{ cm}^{-1}$)]				λ_{em} (nm), room temperature		λ_{em} (nm), 77 K	Φ_{PL} (%)	τ (μs)	k_r^a (μs^{-1})	k_{nr}^a (μs^{-1})
Ir–A3	230 (34)	305 (41)	326 (40)	425 (5.9)	558, 598		548, 594	45	0.25	1.80	2.20
Ir–B	240 (18)	298 (25)	336 (20)	429 (3.5)	563, 600		551, 601	50	0.23	2.17	2.17
Ir–B1	233 (34)	306 (47)	333 (43)	430 (6.9)	563, 600		555, 595	66	0.21	3.14	1.62
Ir–B3	236 (27)	304 (32)	332 (33)	429 (4.9)	563, 600		553, 595	48	0.26	1.85	2.00
Ir–C	234 (25)	297 (34)	334 (26)	429 (4.8)	563, 600		549, 592	47	0.24	1.96	2.21
Ir–C1	234 (31)	307 (43)	330 (40)	428 (6.2)	563, 600		550, 594	52	0.24	2.17	2.00
Ir–C3	234 (35)	305 (40)	332 (42)	427 (6.5)	563, 600		553, 596	66	0.27	2.44	1.26

^aRadiative (k_r) and nonradiative (k_{nr}) decay constants estimated from the measured quantum yields and lifetimes, assuming that the emissive state is formed with unitary efficiency upon excitation.

with liquid crystal properties (vide infra) can self-organize into a helical supramolecular structure. The chirality of the Ir–C3 complex was measured by circular dichroism (CD) in a CH₂Cl₂ solution and liquid-crystalline states. CD signals of the Ir–C3 complex are silent in both CH₂Cl₂ solution and liquid-crystalline phase (Figure S3), indicating that the Ir–C3 complex is a racemic mixture both in solution and in the liquid-crystalline phase.

Electrochemical Properties. To research the charge carrier injection behavior, the electrochemical properties of complexes, taking Ir–B3 and Ir–C3 as representative examples, were measured by cyclic voltammetry (CV) in a 0.1 M Bu₄NPF₆/CH₂Cl₂ solution (Figure S4 and Figure 4).

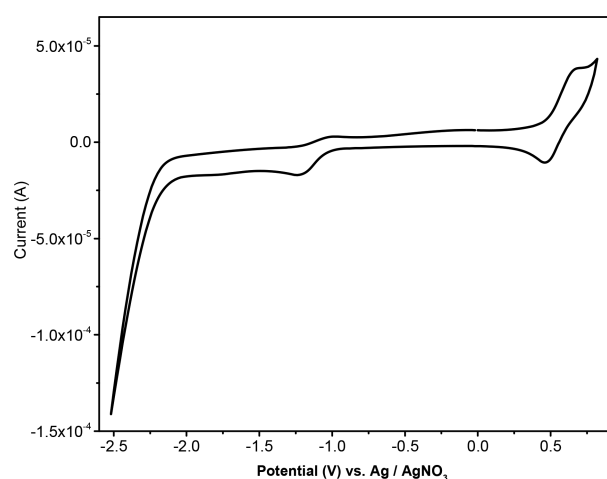


Figure 4. Cyclic voltammetry (CV) of the Ir–C3 complex. CV data were measured in a degassed CH₂Cl₂ solution ($M = 1.0 \times 10^{-3} \text{ mol/L}$) with a Pt wire, a Ag/AgNO₃ electrode, and glassy carbon as the counter, reference, and working electrodes, respectively. The scan rate was 100 mV s^{-1} , and ferrocene was used as a reference.

Ir–B3 and Ir–C3 complexes undergo an irreversible oxidation process with peak potentials at 0.51 and 0.50 V (vs Fc/Fc⁺) for Ir–C3 and Ir–B3, respectively. As reported for the cyclometalated iridium(III) complexes,^{8,53} the oxidation processes are assigned to metal-centered oxidation. The irreversible oxidation characteristic of these complexes suggests that the cyclometalated ligand is greatly involved in the oxidation processes,^{60–63} which is also supported by the results of time-dependent density functional theory (TD-DFT) calculations for Ir–A3 (see below). Meanwhile, Ir–B3 and Ir–C3 also exhibit irreversible reduction waves with reduction waves at -1.44 and -1.40 V (vs Fc/Fc⁺), respectively. The reduction occurs mainly on the ligands, which is attributed to the reduction of ligands via the pyridyltetrazolate moiety.⁵³

Computational Investigation. To further investigate the influence of electronic energy levels and electronic transition characters on the electrochemical and photophysical properties, density function theory (DFT) calculations for a representative complex (Ir–A3) were performed in CH₂Cl₂ solution. The ground state geometry of Ir–A3 was optimized by means of DFT employing the exchange correlation hybrid functional B3LYP-D3, using the 6-311G(d,p) basis set for all nonmetallic elements and the Stuttgart–Dresden (SDD) effective core potential for iridium. The excited states of Ir–A3 were calculated by TD-DFT with the optimized ground state structure. The optimized molecular structure and relevant frontier orbitals for Ir–A3 are shown in Figure 5. The relevant

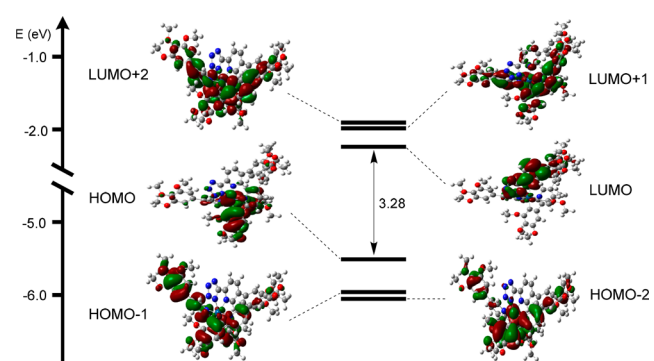


Figure 5. Partial molecular orbital diagram for the Ir–A3 complex with some selected isodensity frontier molecular orbital mainly involved in the electronic transitions. All the DFT energy values are given in electronvolts. The arrows are intended to highlight the HOMO–LUMO energy gaps.

transitions involved along with their energy, oscillator strengths, and character computed in CH₂Cl₂ solutions are listed in Table S4. Compared to those of theory calculations with X-ray diffractometric data, the differences in bond lengths are on the order of picometers (Table S2), indicating that the calculated molecular structure is quite consistent with the geometry obtained by single-crystal X-ray diffractometric analysis. The electrons in the highest occupied molecular orbital (HOMO) are distributed over coordinated phenylpyridine fragments of the main ligands, with a considerable contribution from the d orbital of the central iridium atom, which results in an irreversible oxidation process during electrochemical testing (see above). In contrast, the electrons in the lowest unoccupied orbital (LUMO) are mainly delocalized on the pyridyltetrazolate fragment of the auxiliary ligand with a small contribution of the phenyl ring attached to the pyridine moiety. The delocalized LUMO orbital causes lower LUMO energy level, resulting in red-shifted absorption

and emission spectra for the present iridium(III) complexes compared to those of the analogous pyridyltetrazolate iridium(III) complexes.⁵³

Liquid Crystal Properties. The liquid crystal behavior of these iridium(III) complexes was preliminarily detected by POM and DSC. All complexes show glassy or crystalline states during heating and cooling processes except the Ir–C1 and Ir–C3 complexes; they have 2,5-diphenylpyridine with six alkoxy chains ($n = 12$) and pyridyltetrazolate with alkoxy chains ($n = 12$). For Ir–C1 and Ir–C3 complexes, the typically fan-shaped textures of the hexagonal columnar phase were observed by POM during slow (2 °C/min) heating and cooling processes (Figure S5 and Figure 6). DSC data (Figure

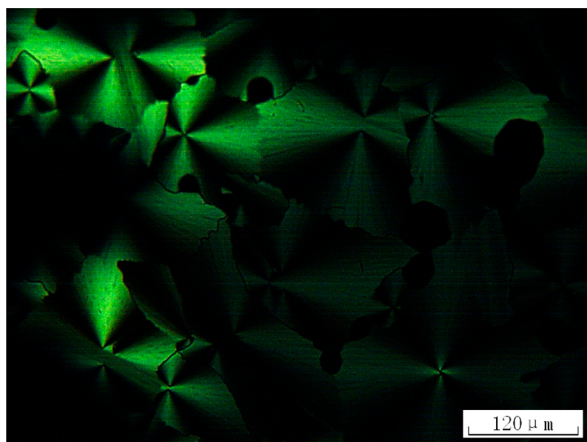


Figure 6. Polarized optical micrographs (on cooling) of the Ir–C3 complex (90 °C).

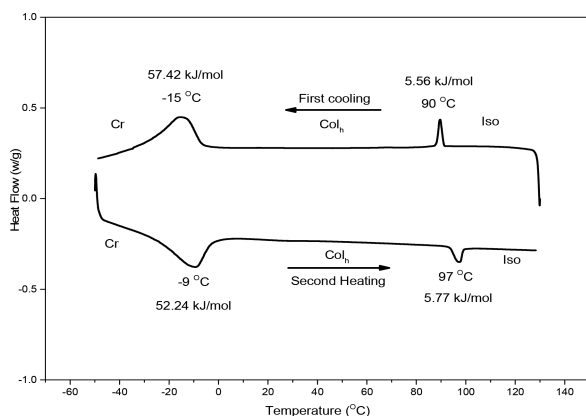


Figure 7. Differential scanning calorimetry curves of the Ir–C3 complex at a scan rate of 10 °C/min under the protection of nitrogen.

7, Figure S6, and Table S5) indicate that both Ir–C1 and Ir–C3 complexes exhibit enantiotropic room-temperature liquid-crystalline behavior. The Ir–C1 complex with one alkoxy chain on pyridyltetrazolate has a lower melting point (–21 °C), a higher clearing point (121 °C), and a wider mesophase range (142 °C) compared to those of the Ir–C3 complex with three alkoxy chains connected to pyridyltetrazolate for which the melting point, clearing point, and mesophase range are –9, 97, and 106 °C, respectively. On the contrary, the Ir–C complex, with six long alkoxy chains ($n = 12$) on the main ligand and no alkoxy chain on the auxiliary ligand, was cooled

directly from the isotropic phase to the crystal phase, indicating that having fewer alkoxy chains is not conducive to the formation of the liquid crystal. The complexes, Ir–B, Ir–B1, and Ir–B3, with shorter alkoxy chains ($n = 6$) on the main ligand and no alkoxy chain, one alkoxy chain, or three alkoxy chains on the auxiliary ligand, reached crystal or glass phases when these complexes cooled, suggesting that overly strong intermolecular interactions (forming a crystal, such as Ir–B3) or overly weak intermolecular interactions (forming a glass, such as Ir–B or Ir–B1) do not favor mesogenic phases. There seems to be a subtle balance between the number and length of alkoxy chains for the formation of liquid crystals.

XRD measurements for Ir–C1 and Ir–C3 further confirm their phase structures clearly. XRD patterns of Ir–C1 and Ir–C3 at 25 °C are shown in Figure S7 and Figure 8, respectively.

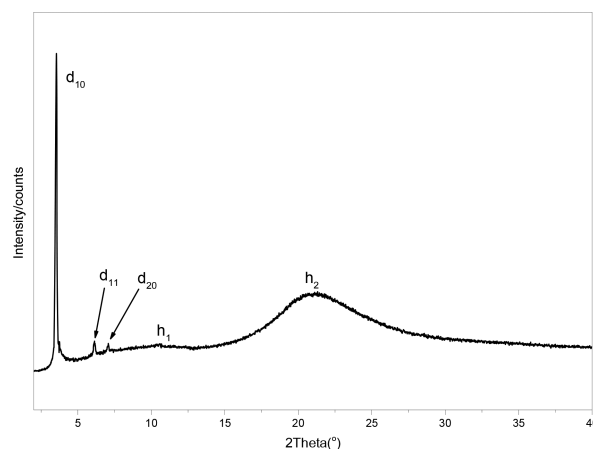


Figure 8. Powder XRD patterns of the Ir–C3 complex at room temperature.

For Ir–C1, there are one intense peak at $2\theta = 3.5^\circ$ and two weak peaks at $2\theta = 6.14^\circ$ and 7.03° in the small-angle region ($2\theta = 2\text{--}12^\circ$); the corresponding d spacing values are 25.22, 14.60, and 12.60 Å, respectively, which are indexed as d_{10} , d_{11} , and d_{20} reflections, respectively. The ratio of their d spacing in reflection peaks is approximately $1:\sqrt{3}:\sqrt{3}/2$, which is consistent with the d spacing value ratio of the hexagonal columnar phase. The distinct halo (h_2) at $2\theta = 21.25^\circ$ ($d = 4.18$ Å) is assigned to liquid-like order between the peripheral alkoxy chains. Moreover, there is an obscure diffuse peak (h_1) at $2\theta = 11.55^\circ$ ($d = 7.66$ Å), which is tentatively attributed to weaker Ir–Ir intermolecular interactions in each column. We note that there is no obvious diffuse peak at ~ 3.5 Å, indicating that there are weaker π – π intermolecular interactions in the columns. Very weak Ir–Ir and π – π intermolecular interactions suggest that the organization within the each column is rather disordered. According to the formula reported in the literature,²¹ the calculated lattice parameter (a) for the hexagonal columnar phase is 29.12 Å. Analogously, for Ir–C3, in the small-angle region three reflection peaks were observed at $2\theta = 3.63^\circ$ (24.25 Å), 6.20° (14.25 Å), and 7.11° (12.43 Å), with a d spacing ratio of $1:\sqrt{3}:\sqrt{3}/2$, and an obscure diffuse peak (h_1) at $2\theta = 11.52^\circ$ ($d = 7.68$ Å) and a distinct diffuse scattering halo (h_2) at $2\theta = 21.20^\circ$ (4.20 Å) also appeared. The calculated lattice parameter (a) for the hexagonal columnar phase is 28.01 Å. XRD measurements indicate that Ir–C1 and Ir–C3 self-organize into the hexagonal columnar phase, and the

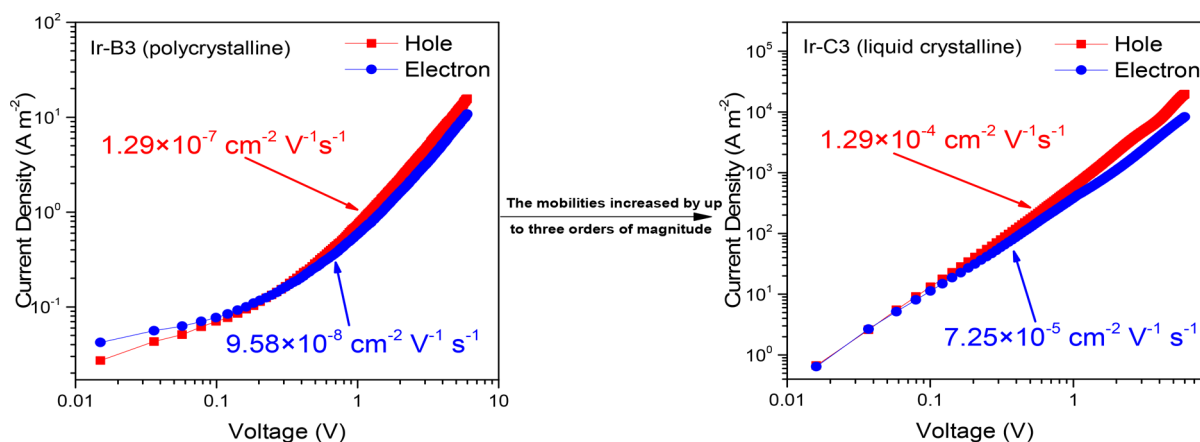


Figure 9. I - V curves of the hole and electron for Ir-B3 (left) and Ir-C3 (right).

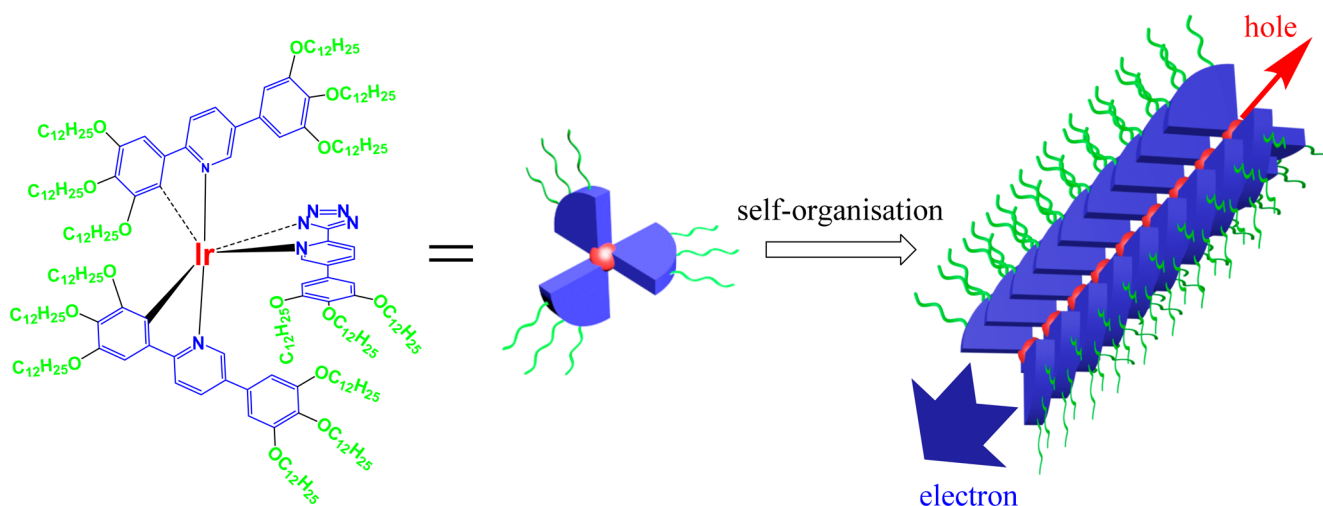


Figure 10. Model structure of the Ir-C3 complex and its self-organization into nanostructure for ambipolar conductive columnar materials.

complexes are loosely packed within the columns due to weaker Ir-Ir and π - π intermolecular interactions.

Ambipolar Carrier Transport Properties. During the application of organic semiconductors, such as OLEDs, organic field-effect transistors (OFETs), and organic photovoltaic devices (OPVs), the charge carrier mobility, especially the well-balanced ambipolar mobility, is considered to be crucial to achieving high device performances.^{18,64–67} To achieve ambipolar transporting properties in a molecular structure, the molecule would be composed of electron-transporting chromophores (electron acceptor groups) and hole-transporting chromophores (electron donor groups). However, the carrier mobilities of the material depend not only on the molecules themselves but also on the modes of molecular packing. For example, in the polycrystalline phase, well-ordered packing facilitates the charge transport between neighboring molecules, but grain boundaries interrupt the carrier transporting process. On the other hand, because of poor local order and weak π -orbital overlap between molecules, amorphous films display an unsatisfactory charge-transfer property.⁶⁸ Compared to polycrystalline and amorphous states, the lower level of positional order in liquid crystal systems makes liquid crystal molecules have a weaker tendency to form structural defects and multidomains with the grain boundaries so that liquid crystal molecules tend to self-organize into the

homogeneously ordered domains with large areas, resulting in improved charge mobility.⁶⁹

Electron mobilities (μ_e) and hole mobilities (μ_h) of complexes Ir-B3 and Ir-C3 were measured at room temperature using the space charge limited-current (SCLC) method. The hole-only devices were fabricated with a glass/ITO/PEDOT:PSS/Ir-B3 (or Ir-C3)/MoO₃/Au structure, and the electron mobility devices were fabricated with a glass/Al/Ir-B3 (or Ir-C3)/Al structure. Devices were fabricated by a conventional method, except that when the active layer of Ir-B3 or Ir-C3 was spin coated on the substrate, the substrate was heated to 150 °C for 5 min and then cooled slowly (5 °C/min) to room temperature to obtain homogeneous films. The current-voltage (I - V) curves and the detailed mobility data are shown in Figure 9. As expected, the devices based on a polycrystalline film of Ir-B3 display very low hole and electron mobilities of 1.29×10^{-7} and $9.58 \times 10^{-8} \text{ cm}^2 \text{ V}^{-1} \text{ s}^{-1}$, respectively. On the contrary, the devices, based on liquid crystal films of Ir-C3 that are assumed to form one-dimensional (1D) columnar structures, display improved hole and electron mobilities of 1.29×10^{-4} and $7.25 \times 10^{-5} \text{ cm}^2 \text{ V}^{-1} \text{ s}^{-1}$, respectively. In addition, the hole mobility of Ir-C3 is higher than that of the relevant platinum(II) complex ($6.30 \times 10^{-5} \text{ cm}^2 \text{ V}^{-1} \text{ s}^{-1}$),⁴⁴ indicating that the 1D columnar structure is beneficial to the transmission of holes. Conversely, the electron mobility of Ir-C3 is lower than that of the

relevant platinum(II) complex ($3.30 \times 10^{-4} \text{ cm}^{-2} \text{ V}^{-1} \text{ s}^{-1}$), which should be attributed to the very weak π - π interactions of Ir-C3 in 1D columnar structures. The $\mu_{\text{h}}/\mu_{\text{e}}$ value for Ir-C3 is 1.71, indicating that Ir-C3 exhibits ambipolar carrier transport behavior. We suppose that hole transport is related to the central metal ions of the complexes, because of their multiple oxidation states and low kinetic barriers for self-exchange reactions,⁷⁰⁻⁷³ and peripheral pyridyltetrazolate co-ligands with a strong electron affinity that act as an electron acceptor are responsible for electron transport. Moreover, the ambipolar charge mobilities are greatly improved in the hexagonal columnar phase because of the 1D columnar structure. On the other hand, the carrier mobilities in the columnar mesogenic phase are even lower than that reported in some columnar liquid crystals,^{18,20,21} which indicates that the somewhat disordered molecular organization in the columns (as discussed above) is not conducive to carrier transport. For these iridium(III) liquid crystal complexes with the distorted octahedral structure, it is very difficult to represent an accurate mode for their molecular self-organization, considering the many possibilities of their arrangement into columnar phases.^{59,74,75} Here, we present the hypothetical self-organization model (Figure 10). In the mesogenic phase, an individual molecule can self-organize into 1D columnar structures driven by weaker intermolecular interactions. In the columnar phase, the iridium center and peripheral ligands form a rather ordered 1D hole and electron channel, which is beneficial for the transportation of the carrier. The outermost long alkoxyl chains separate the columnar units and act as an insulator.

CONCLUSION

In conclusion, we demonstrate that 1D columnar structures of iridium(III) metallomesogens with ambipolar charge mobility behavior can be formed by introducing polycatenar 2,5-diphenylpyridine and pyridyltetrazolate derivatives. With a higher PL quantum yield and ambipolar mobility and liquid-crystalline property, these iridium(III) metallomesogens may be used as multifunctional semiconductor materials.

ASSOCIATED CONTENT

Supporting Information

The Supporting Information is available free of charge on the ACS Publications website at DOI: 10.1021/acs.inorgchem.8b02984.

Materials and methods; synthesis and characterization, including NMR spectra and elemental analysis of iridium(III) complexes; tables of crystallographic data and selected bond lengths and angles of Ir-A3; phosphorescence decays, PL, DSC spectra, and detailed data; cyclic voltammograms of Ir-B3 and polarized optical micrographs of Ir-C1; a table of computed excitation energies and oscillator strengths for the $S_0 \rightarrow S_n$ transitions of Ir-A3 (PDF)

Accession Codes

CCDC 1588649 contains the supplementary crystallographic data for this paper. These data can be obtained free of charge via www.ccdc.cam.ac.uk/data_request/cif, or by emailing data_request@ccdc.cam.ac.uk, or by contacting The Cambridge Crystallographic Data Centre, 12 Union Road, Cambridge CB2 1EZ, UK; fax: +44 1223 336033.

AUTHOR INFORMATION

Corresponding Author

*E-mail: luo-k-j007@163.com.

ORCID

Kaijun Luo: 0000-0003-1636-3028

Notes

The authors declare no competing financial interest.

ACKNOWLEDGMENTS

The authors are grateful for the financial support from the National Natural Science Foundation of China (21172161 and 21072147) and the Laboratory and Equipment Management Department of Sichuan Normal University (DJGX2017007). The authors are also grateful for the contributions of Qiang Peng and Xiaopeng Xu to device fabrication and measurements.

REFERENCES

- (1) Xiao, L.; Chen, Z.; Qu, B.; Luo, J.; Kong, S.; Gong, Q.; Kido, J. Recent Progresses on Materials for Electrophosphorescent Organic Light-Emitting Devices. *Adv. Mater.* **2011**, *23*, 926–952.
- (2) Li, K.; Ming Tong, G. S.; Wan, Q.; Cheng, G.; Tong, W. Y.; Ang, W. H.; Kwong, W. L.; Che, C. M. Highly Phosphorescent Platinum(II) Emitters: Photophysics, Materials and Biological Applications. *Chem. Sci.* **2016**, *7*, 1653–1673.
- (3) Kong, F. K.; Tang, M. C.; Wong, Y. C.; Chan, M. Y.; Yam, V. W. Design Strategy for High-Performance Dendritic Carbazole-Containing Alkynylplatinum(II) Complexes and Their Application in Solution-Processable Organic Light-Emitting Devices. *J. Am. Chem. Soc.* **2016**, *138*, 6281–6291.
- (4) Choy, W. C.; Chan, W. K.; Yuan, Y. Recent Advances in Transition Metal Complexes and Light-Management Engineering in Organic Optoelectronic Devices. *Adv. Mater.* **2014**, *26*, 5368–5398.
- (5) Tamayo, A. B.; Alleyne, B. D.; Djurovich, P. I.; Lamansky, S.; Tsyba, I.; Ho, N. N.; Bau, R.; Thompson, M. E. Synthesis and Characterization of Facial and Meridional Tris-cyclometalated Iridium(III) Complexes. *J. Am. Chem. Soc.* **2003**, *125*, 7377–7387.
- (6) Graber, S.; Doyle, K.; Neuburger, M.; Housecroft, C. E.; Constable, E. C.; Costa, R. D.; Ortí, E.; Repetto, D.; Bolink, H. J. A Supramolecularly-Caged Ionic Iridium(III) Complex Yielding Bright and Very Stable Solid-State Light-Emitting Electrochemical Cells. *J. Am. Chem. Soc.* **2008**, *130*, 14944–14945.
- (7) Cui, L.-S.; Liu, Y.; Liu, X.-Y.; Jiang, Z.-Q.; Liao, L.-S. Design and Synthesis of Pyrimidine-Based Iridium(III) Complexes with Horizontal Orientation for Orange and White Phosphorescent OLEDs. *ACS Appl. Mater. Interfaces* **2015**, *7*, 11007–11014.
- (8) Benjamin, H.; Zheng, Y.; Batsanov, A. S.; Fox, M. A.; Al-Attar, H. A.; Monkman, A. P.; Bryce, M. R. Sulfonyl-Substituted Heteroleptic Cyclometalated Iridium(III) Complexes as Blue Emitters for Solution-Processable Phosphorescent Organic Light-Emitting Diodes. *Inorg. Chem.* **2016**, *55*, 8612–8627.
- (9) Chi, Y.; Chou, P.-T. Transition-Metal Phosphors with Cyclometalating Ligands: Fundamentals and Applications. *Chem. Soc. Rev.* **2010**, *39*, 638–655.
- (10) Yang, C.-H.; Beltran, J.; Lemaure, V.; Cornil, J.; Hartmann, D.; Sarfert, W.; Fröhlich, R.; Bizzarri, C.; De Cola, L. Iridium Metal Complexes Containing N-Heterocyclic Carbene Ligands for Blue-Light-Emitting Electrochemical Cells. *Inorg. Chem.* **2010**, *49*, 9891–9901.
- (11) Zysman-Colman, E.; Slinker, J. D.; Parker, J. B.; Malliaras, G. G.; Bernhard, S. Improved Turn-On Times of Light-Emitting Electrochemical Cells. *Chem. Mater.* **2008**, *20*, 388–396.
- (12) Kang, J. H.; Kim, H. J.; Kwon, T.-H.; Hong, J.-I. Phosphorescent Sensor for Phosphorylated Peptides Based on an Iridium Complex. *J. Org. Chem.* **2014**, *79*, 6000–6005.

- (13) Geldmacher, Y.; Kitanovic, I.; Alborzina, H.; Bergerhoff, K.; Rubbiani, R.; Wefelmeier, P.; Prokop, A.; Gust, R.; Ott, I.; Wöfl, S.; Sheldrick, W. S. Cellular Selectivity and Biological Impact of Cytotoxic Rhodium(III) and Iridium(III) Complexes Containing Methyl-Substituted Phenanthroline Ligands. *ChemMedChem* **2011**, *6*, 429–439.
- (14) Zhao, Q.; Huang, C.; Li, F. Phosphorescent Heavy-Metal Complexes for Bioimaging. *Chem. Soc. Rev.* **2011**, *40*, 2508–2524.
- (15) Zhang, G.; Zhang, H.; Gao, Y.; Tao, R.; Xin, L.; Yi, J.; Li, F.; Liu, W.; Qiao, J. Near-Infrared-Emitting Iridium(III) Complexes as Phosphorescent Dyes for Live Cell Imaging. *Organometallics* **2014**, *33*, 61–68.
- (16) Zhou, Y.; Jia, J.; Li, W.; Fei, H.; Zhou, M. Luminescent Biscarbene Iridium(III) Complexes as Living Cell Imaging Reagents. *Chem. Commun.* **2013**, *49*, 3230–3232.
- (17) Maity, A.; Choi, J. S.; Teets, T. S.; Deligonul, N.; Berdis, A. J.; Gray, T. G. Cyclometalated Iridium(III) Complexes with Deoxyribose Substituents. *Chem. - Eur. J.* **2013**, *19*, 15924–15932.
- (18) Wohrle, T.; Wurzbach, I.; Kirres, J.; Kostidou, A.; Kapernaum, N.; Litterscheidt, J.; Haenle, J. C.; Staffeld, P.; Baro, A.; Giesselmann, F.; Laschat, S. Discotic Liquid Crystals. *Chem. Rev.* **2016**, *116*, 1139–1241.
- (19) Kozhevnikov, V. N.; Donnio, B.; Heinrich, B.; Bruce, D. W. Morphology-Driven Absorption and Emission Colour Changes in Liquid-Crystalline, Cyclometalated Platinum(II) Complexes. *Chem. Commun.* **2014**, *50*, 14191–14193.
- (20) Concellon, A.; Marcos, M.; Romero, P.; Serrano, J. L.; Termine, R.; Golemme, A. Not Only Columns: High Hole Mobility in a Discotic Nematic Mesophase Formed by Metal-Containing Porphyrin-Core Dendrimers. *Angew. Chem., Int. Ed.* **2017**, *56*, 1259–1263.
- (21) Laschat, S.; Baro, A.; Steinke, N.; Giesselmann, F.; Hagele, C.; Scalia, G.; Judele, R.; Kapatsina, E.; Sauer, S.; Schreivogel, A.; Tosoni, M. Discotic Liquid Crystals: From Tailor-Made Synthesis to Plastic Electronics. *Angew. Chem., Int. Ed.* **2007**, *46*, 4832–4887.
- (22) Krikorian, M.; Liu, S.; Swager, T. M. Columnar Liquid Crystallinity and Mechanochromism in Cationic Platinum(II) Complexes. *J. Am. Chem. Soc.* **2014**, *136*, 2952–2955.
- (23) Kozhevnikov, V. N.; Donnio, B.; Bruce, D. W. Phosphorescent, Terdentate, Liquid-Crystalline Complexes of Platinum(II): Stimulus-Dependent Emission. *Angew. Chem., Int. Ed.* **2008**, *47*, 6286–6289.
- (24) Spencer, M.; Santoro, A.; Freeman, G. R.; Diez, A.; Murray, P. R.; Torroba, J.; Whitwood, A. C.; Yellowlees, L. J.; Williams, J. A.; Bruce, D. W. Phosphorescent, Liquid-Crystalline Complexes of Platinum(II): Influence of the Beta-Diketonate Co-igand on Mesomorphism and Emission Properties. *Dalton Trans* **2012**, *41*, 14244–14256.
- (25) Yam, V. W.; Au, V. K.; Leung, S. Y. Light-Emitting Self-Assembled Materials Based on d(8) and d(10) Transition Metal Complexes. *Chem. Rev.* **2015**, *115*, 7589–7728.
- (26) Cuerva, C.; Campo, J. A.; Cano, M.; Lodeiro, C. Platinum(II) Metallomesogens: New External-Stimuli-Responsive Photoluminescence Materials. *Chem. - Eur. J.* **2016**, *22*, 10168–10178.
- (27) Wang, Y.; Liu, Y.; Luo, J.; Qi, H.; Li, X.; Nin, M.; Liu, M.; Shi, D.; Zhu, W.; Cao, Y. Metallomesogens based on Platinum(II) Complexes: Synthesis, Luminescence and Polarized Emission. *Dalton Trans* **2011**, *40*, 5046–5051.
- (28) Zhang, S.; Luo, K.; Geng, H.; Ni, H.; Wang, H.; Li, Q. New Phosphorescent Platinum(II) Complexes with Tetradentate C^{*}N^{*}N^{*}C Ligands: Liquid Crystallinity and Polarized Emission. *Dalton Trans* **2017**, *46*, 899–906.
- (29) Chang, H.-C.; Shiozaki, T.; Kamata, A.; Kishida, K.; Ohmori, T.; Kiriya, D.; Yamauchi, T.; Furukawa, H.; Kitagawa, S. A Redox-active Columnar Metallomesogen and Its Cyclic Voltammetric Responses. *J. Mater. Chem.* **2007**, *17*, 4136–4138.
- (30) Santoro, A.; Whitwood, A. C.; Williams, J. A. G.; Kozhevnikov, V. N.; Bruce, D. W. Synthesis, Mesomorphism, and Luminescent Properties of Calamitic 2-Phenylpyridines and Their Complexes with Platinum(II). *Chem. Mater.* **2009**, *21*, 3871–3882.
- (31) Chico, R.; de Domingo, E.; Domínguez, C.; Donnio, B.; Heinrich, B.; Termine, R.; Golemme, A.; Coco, S.; Espinet, P. High One-Dimensional Charge Mobility in Semiconducting Columnar Mesophases of Isocyano-Triphenylene Metal Complexes. *Chem. Mater.* **2017**, *29*, 7587–7595.
- (32) Wu, X.; Zhu, M.; Bruce, D. W.; Zhu, W.; Wang, Y. An Overview of Phosphorescent Metallomesogens based on Platinum and Iridium. *J. Mater. Chem. C* **2018**, *6*, 9848–9860.
- (33) Santoro, A.; Wegrzyn, M.; Whitwood, A. C.; Donnio, B.; Bruce, D. W. Oxidation of Organoplatinum(II) by Coordinated Dimethylsulfoxide: Metal-Metal Bonded, Dinuclear, Liquid-Crystalline Complexes of Platinum(III). *J. Am. Chem. Soc.* **2010**, *132*, 10689–10691.
- (34) Venkatesan, K.; Kouwer, P. H. J.; Yagi, S.; Müller, P.; Swager, T. M. Columnar Mesophases from Half-Discoid Platinum Cyclo-metalated Metallomesogens. *J. Mater. Chem.* **2008**, *18*, 400–407.
- (35) Wang, Y.; Chen, Q.; Li, Y.; Liu, Y.; Tan, H.; Yu, J.; Zhu, M.; Wu, H.; Zhu, W.; Cao, Y. Highly Dichroic Metallomesogen of Dinuclear Platinum Complex: Synthesis and Liquid Crystal and Photophysical Properties. *J. Phys. Chem. C* **2012**, *116*, 5908–5914.
- (36) Zou, G.; Luo, K.; Zhao, L.; Ni, H.; Wang, H.; Li, Q. Ortho-Platinated Metallomesogens based on Rod Mesogenic Unit of 2-phenylpyridine Derivatives: Synthesis, High Linearly Polarized and Phase-State-Dependent Luminescence. *Liq. Cryst.* **2018**, *45*, 593–606.
- (37) Pucci, D.; Donnio, B. *Handbook of Liquid Crystals*; Wiley-VCH, 2014.
- (38) Lin, C.-J.; Liu, Y.-H.; Peng, S.-M.; Shinmyozu, T.; Yang, J.-S. Excimer-Monomer Photoluminescence Mechanochromism and Vapochromism of Pentiptycene-Containing Cyclometalated Platinum(II) Complexes. *Inorg. Chem.* **2017**, *56*, 4978–4989.
- (39) Williams, J. A. G.; Develay, S.; Rochester, D.; Murphy, L. Optimising the Luminescence of Platinum(II) Complexes and Their Application in Organic Light Emitting Devices (OLEDs). *Coord. Chem. Rev.* **2008**, *252*, 2596–2611.
- (40) Szerb, E. I.; Talarico, A. M.; Aiello, I.; Crispini, A.; Godbert, N.; Pucci, D.; Pugliese, T.; Ghedini, M. Red to Green Switch Driven by Order in an Ionic Ir^{III} Liquid-Crystalline Complex. *Eur. J. Inorg. Chem.* **2010**, *2010*, 3270–3277.
- (41) Santoro, A.; Prokhorov, A. M.; Kozhevnikov, V. N.; Whitwood, A. C.; Donnio, B.; Williams, J. A. G.; Bruce, D. W. Emissive Metallomesogens Based on 2-Phenylpyridine Complexes of Iridium(III). *J. Am. Chem. Soc.* **2011**, *133*, 5248–5251.
- (42) Prokhorov, A. M.; Santoro, A.; Williams, J. A. G.; Bruce, D. W. Phosphorescent Mesomorphic Dyads Based on Tetraacetylene Complexes of Iridium(III). *Angew. Chem., Int. Ed.* **2012**, *51*, 95–98.
- (43) Wang, Y.; Cabry, C. P.; Xiao, M.; Male, L.; Cowling, S. J.; Bruce, D. W.; Shi, J.; Zhu, W.; Baranoff, E. Blue and Green Phosphorescent Liquid-Crystalline Iridium Complexes with High Hole Mobility. *Chem. - Eur. J.* **2016**, *22*, 1618–1621.
- (44) Geng, H.; Luo, K.; Zou, G.; Zhao, L.; Wang, H.; Li, Q.; Ni, H. Have Ambipolar Carrier Transmission Property based on Novel Platinum(II) Complexes: Synthesis, Photophysical Properties, Liquid Crystalline Characteristics, Polarized Luminescence. *Dyes Pigm.* **2018**, *149*, 82–91.
- (45) McManus, J. M.; Herbst, R. M. Tetrazole Analogs of Pyridinecarboxylic Acids. *J. Org. Chem.* **1959**, *24*, 1462–1464.
- (46) Wallace, L.; Rillema, D. P. Photophysical Properties of Rhenium(I) Tricarbonyl Complexes Containing Alkyl- and Aryl-Substituted Phenanthrolines as Ligands. *Inorg. Chem.* **1993**, *32*, 3836–3843.
- (47) Palatinus, L.; Prathapa, S. J.; van Smaalen, S. EDMA: A Computer Program for Topological Analysis of Discrete Electron Densities. *J. Appl. Crystallogr.* **2012**, *45*, 575–580.
- (48) Dolomanov, O. V.; Bourhis, L. J.; Gildea, R. J.; Howard, J. A. K.; Puschmann, H. OLEX2: A Complete Structure Solution, Refinement and Analysis Program. *J. Appl. Crystallogr.* **2009**, *42*, 339–341.
- (49) Sheldrick, G. M. A Short History of SHELX. *Acta Crystallogr., Sect. A: Found. Crystallogr.* **2008**, *64*, 112–122.

- (50) Feng, K.; Yang, G.; Xu, X.; Zhang, G.; Yan, H.; Awartani, O.; Ye, L.; Ade, H.; Li, Y.; Peng, Q. High-Performance Wide Bandgap Copolymers Using an EDOT Modified Benzodithiophene Donor Block with 10.11% Efficiency. *Adv. Energy Mater.* **2018**, *8*, 1602773–1602780.
- (51) Duan, Y.; Xu, X.; Yan, H.; Wu, W.; Li, Z.; Peng, Q. Pronounced Effects of a Triazine Core on Photovoltaic Performance—Efficient Organic Solar Cells Enabled by a PDI Trimer-Based Small Molecular Acceptor. *Adv. Mater.* **2017**, *29*, 1605115–1605120.
- (52) Wu, L.-L.; Yang, C.-H.; Sun, I. W.; Chu, S.-Y.; Kao, P.-C.; Huang, H.-H. Photophysical and Electrochemical Properties of Blue Phosphorescent Iridium(III) Complexes. *Organometallics* **2007**, *26*, 2017–2023.
- (53) Stagni, S.; Colella, S.; Palazzi, A.; Valenti, G.; Zacchini, S.; Paolucci, F.; Marcaccio, M.; Albuquerque, R. Q.; De Cola, L. Essential Role of the Ancillary Ligand in the Color Tuning of Iridium Tetrazolate Complexes. *Inorg. Chem.* **2008**, *47*, 10509–10521.
- (54) Lamansky, S.; Djurovich, P.; Murphy, D.; Abdel-Razzaq, F.; Lee, H.-E.; Adachi, C.; Burrows, P. E.; Forrest, S. R.; Thompson, M. E. Highly Phosphorescent Bis-Cyclometalated Iridium Complexes: Synthesis, Photophysical Characterization, and Use in Organic Light Emitting Diodes. *J. Am. Chem. Soc.* **2001**, *123*, 4304–4312.
- (55) Kozhevnikov, V. N.; Durrant, M. C.; Williams, J. A. G. Highly Luminescent Mixed-Metal Pt(II)/Ir(III) Complexes: Bis-Cyclometalation of 4,6-Diphenylpyrimidine As a Versatile Route to Rigid Multimetallic Assemblies. *Inorg. Chem.* **2011**, *50*, 6304–6313.
- (56) Lamansky, S.; Djurovich, P.; Murphy, D.; Abdel-Razzaq, F.; Kwong, R.; Tsyba, I.; Bortz, M.; Mui, B.; Bau, R.; Thompson, M. E. Synthesis and Characterization of Phosphorescent Cyclometalated Iridium Complexes. *Inorg. Chem.* **2001**, *40*, 1704–1711.
- (57) Yang, C.-H.; Mauro, M.; Polo, F.; Watanabe, S.; Muenster, I.; Fröhlich, R.; De Cola, L. Deep-Blue-Emitting Heteroleptic Iridium(III) Complexes Suited for Highly Efficient Phosphorescent OLEDs. *Chem. Mater.* **2012**, *24*, 3684–3695.
- (58) Liu, M.; Zhang, L.; Wang, T. Supramolecular Chirality in Self-Assembled Systems. *Chem. Rev.* **2015**, *115*, 7304–7397.
- (59) Li, T.-Y.; Jing, Y.-M.; Liu, X.; Zhao, Y.; Shi, L.; Tang, Z.; Zheng, Y.-X.; Zuo, J.-L. Circularly Polarised Phosphorescent Photoluminescence and Electroluminescence of Iridium Complexes. *Sci. Rep.* **2015**, *5*, 14912–14920.
- (60) Zhao, Q.; Liu, S.; Shi, M.; Wang, C.; Yu, M.; Li, L.; Li, F.; Yi, T.; Huang, C. Series of New Cationic Iridium(III) Complexes with Tunable Emission Wavelength and Excited State Properties: Structures, Theoretical Calculations, and Photophysical and Electrochemical Properties. *Inorg. Chem.* **2006**, *45*, 6152–6160.
- (61) Didier, P.; Ortman, I.; Kirsch-De Mesmaeker, A.; Watts, R. J. Electrochemistry and Absorption and Emission Spectroscopy of New Orthometalated Complexes of Rhodium(III) and Iridium(III) with the Ligands 1,4,5,8-tetraazaphenanthrene and 1, 4, 5, 8, 9, 12-hexaazatriphenylene. *Inorg. Chem.* **1993**, *32*, 5239–5245.
- (62) Calogero, G.; Giuffrida, G.; Serroni, S.; Ricevuto, V.; Campagna, S. Absorption Spectra, Luminescence Properties, and Electrochemical Behavior of Cyclometalated Iridium(III) and Rhodium(III) Complexes with a Bis(pyridyl)triazole Ligand. *Inorg. Chem.* **1995**, *34*, 541–545.
- (63) Dragonetti, C.; Falcicola, L.; Mussini, P.; Righetto, S.; Roberto, D.; Ugo, R.; Valore, A.; De Angelis, F.; Fantacci, S.; Sgamellotti, A.; Ramon, M.; Muccini, M. The Role of Substituents on Functionalized 1,10-Phenanthroline in Controlling the Emission Properties of Cationic Iridium(III) Complexes of Interest for Electroluminescent Devices. *Inorg. Chem.* **2007**, *46*, 8533–8547.
- (64) Ostroverkhova, O. Organic Optoelectronic Materials: Mechanisms and Applications. *Chem. Rev.* **2016**, *116*, 13279–13412.
- (65) O'Neill, M.; Kelly, S. M. Ordered Materials for Organic Electronics and Photonics. *Adv. Mater.* **2011**, *23*, 566–584.
- (66) Mei, J.; Ogawa, K.; Kim, Y.-G.; Heston, N. C.; Arenas, D. J.; Nasrollahi, Z.; McCarley, T. D.; Tanner, D. B.; Reynolds, J. R.; Schanze, K. S. Low-Band-Gap Platinum Acetylide Polymers as Active Materials for Organic Solar Cells. *ACS Appl. Mater. Interfaces* **2009**, *1*, 150–161.
- (67) Clem, T. A.; Kavulak, D. F. J.; Westling, E. J.; Fréchet, J. M. J. Cyclometalated Platinum Polymers: Synthesis, Photophysical Properties, and Photovoltaic Performance. *Chem. Mater.* **2010**, *22*, 1977–1987.
- (68) Sun, Y.; Duan, L.; Wei, P.; Qiao, J.; Dong, G.; Wang, L.; Qiu, Y. An Ambipolar Transporting Naphtho[2,3-c][1,2,5]thiadiazole Derivative with High Electron and Hole Mobilities. *Org. Lett.* **2009**, *11*, 2069–2072.
- (69) Pisula, W.; Zorn, M.; Chang, J. Y.; Müllen, K.; Zentel, R. Liquid Crystalline Ordering and Charge Transport in Semiconducting Materials. *Macromol. Rapid Commun.* **2009**, *30*, 1179–1202.
- (70) Ren, X.; Alleyne, B. D.; Djurovich, P. I.; Adachi, C.; Tsyba, I.; Bau, R.; Thompson, M. E. Organometallic Complexes as Hole-Transporting Materials in Organic Light-Emitting Diodes. *Inorg. Chem.* **2004**, *43*, 1697–1707.
- (71) Marcus, R. A. Generalization of Activated-Complex Theory. III. Vibrational Adiabaticity, Separation of Variables, and a Connection with Analytical Mechanics. *J. Chem. Phys.* **1965**, *43*, 1598–1605.
- (72) Newton, M. D.; Sutin, N. Electron Transfer Reactions in Condensed Phases. *Annu. Rev. Phys. Chem.* **1984**, *35*, 437–480.
- (73) Marcus, R. A.; Sutin, N. Electron transfers in chemistry and biology. *Biochim. Biophys. Acta, Rev. Bioenerg.* **1985**, *811*, 265–322.
- (74) Crassous, J. Chiral transfer in coordination complexes: towards molecular materials. *Chem. Soc. Rev.* **2009**, *38*, 830–845.
- (75) Barberá, J.; Caveró, E.; Lehmann, M.; Serrano, J.-L.; Sierra, T.; Vázquez, J. T. Supramolecular Helical Stacking of Metallomesogens Derived from Enantiopure and Racemic Polycatenar Oxazolines. *J. Am. Chem. Soc.* **2003**, *125*, 4527–4533.